Finite size and intrinsic field effect on the polar-active properties of ferroelectric-semiconductor heterostructures

A. N. Morozovska,[1,*] E. A. Eliseev,[1,2] S. V. Svechnikov,[1] A. D. Krutov,[1,3] V. Y. Shur,[4] A. Y. Borisevich,[5] P. Maksymovych,[5] and S. V. Kalinin[5,†]

[1]*Institute of Semiconductor Physics, National Academy of Sciences of Ukraine, 03028 Kiev, Ukraine*
[2]*Institute for Problems of Materials Science, National Academy of Sciences of Ukraine, 03142 Kiev, Ukraine*
[3]*Taras Shevchenko National University of Kyiv, 01033 Kiev, Ukraine*
[4]*Institute of Physics and Applied Mathematics, Ural State University, 620083 Ekaterinburg, Russia*
[5]*Oak Ridge National Laboratory, Oak Ridge, Tennessee 37831, USA*

(Received 31 December 2009; revised manuscript received 12 March 2010; published 7 May 2010)

Using Landau-Ginzburg-Devonshire approach we calculated the equilibrium distributions of electric field, polarization, and space charge in the ferroelectric-semiconductor heterostructures containing proper or incipient ferroelectric thin films. The role of the polarization gradient and intrinsic surface energy, interface dipoles, and free charges on polarization dynamics are specifically explored. The intrinsic field effects, which originated at the ferroelectric-semiconductor interface, lead to the surface band bending and result into the formation of depletion space-charge layer near the semiconductor surface. During the local polarization reversal (caused by the electric field of the nanosized tip of the scanning probe microscope) the thickness and charge of the interface layer drastically changes, in particular, the sign of the screening carriers is determined by the polarization direction. Obtained analytical solutions could be extended to analyze polarization-mediated electronic transport.

DOI: 10.1103/PhysRevB.81.205308 PACS number(s): 77.55.fp, 73.20.At, 73.30.+y, 77.80.B−

I. INTRODUCTION

Polar discontinuity at the interfaces induced either by translational symmetry breaking of a ferroelectric material or ionic-charge mismatch between the components can produce intriguing modification of the interfacial electronic states and polarization of the adjacent materials.[1–4] The representative interfacial phenomena arising from the interplay between polarity and electronic structure include two-dimensional electron gases at the interface of band ($LaAlO_3/SrTiO_3$) (Ref. 2) or band and Mott insulators[5] and polarization-controlled electron tunneling across ferroelectric-semiconductor or half-metal interfaces ($PbTiO_3/(La,Sr)MnO_3$, $BaTiO_3/SrRuO_3$).[6–9] These novel physical phenomena emerging in oxide materials at the nanometer scale hold strong potential for novel devices. Correspondingly, the theoretical insight into the epitaxial interfaces of normal and incipient ferroelectrics with half-metals and semiconductors and interplay between atomistic phenomena at interfaces, mesoscopic potential, and field distributions is acutely needed.

As an illustrative example, the notorious problem of the Schottky barrier in ferroelectric films is still widely debated, with the key question of whether sub-100-nm films are fully depleted, or that the width of the depletion regions is in the sub-10-nm range due to the overall high density $>10^{20}$ cm^{-3} of shallow and deep donor and/or acceptor levels in the film, and particularly in the interfacial regions.[10] More importantly, only several previous works, such as the concept of a ferroelectric Schottky diode[11] and the dielectric nonlinearities in the epitaxial piezoelectric transducer films,[12,13] have emphasized the effect of space-charge layers on polarization distribution and domain-switching dynamics inside ferroelectric films.

In the current paper we present analytical calculations of the polar-active properties (including local polarization reversal) in the proper and incipient ferroelectric-dielectric thin films within Landau-Ginzburg-Devonshire (LGD) phenomenological approach with a special attention to the polarization gradient and intrinsic surface energy, interface dipoles, and free charges. We analyzed the influence of finite-size effect on the intrinsic electric field and polar-active properties of the ferroelectric-semiconductor heterostructures. Although the stability of the spontaneous polarization in the system ferroelectric film /insulator/semiconductor was previously studied within LGD approach,[14] the band structure of the system, interface charges and dipoles, and the polarization gradient and intrinsic surface energy of ferroelectric film were previously ignored. Hence, this work provides a framework to link the mesoscopic LGD-semiconductor theory to the first-principles calculations that can reveal the details of the electrostatic field structure at the interface.

The paper is organized as follows. After stating the problem in Sec. II, analytical solutions for polarization, electric potential, and field and space charge distributions in the model heterostructure are presented in the Secs. III A and III B. The results of the stable ground-state calculations for $SrTiO_3/(La,Sr)MnO_3$ (STO/LSMO) and $BiFeO_3/(La,Sr)MnO_3$ (BFO/LSMO) heterostructures are presented the Sec. III C. Metastable states are considered in Sec. III D. The effect of the incomplete screening and interface charge on the local polarization reversal and domain formation caused by the electric field of the scanning probe microscope (SPM) tip is studied in the Sec. IV. The tunneling current density is estimated, providing an analytical approach to quantify recent experimental measurements of polarization-controlled tunneling.[6–9]

II. PROBLEM STATEMENT

Here we consider an asymmetric heterostructure consisting of a narrow-gap (or metallic) semiconductor and a thin

 ©2010 The American Physical Society

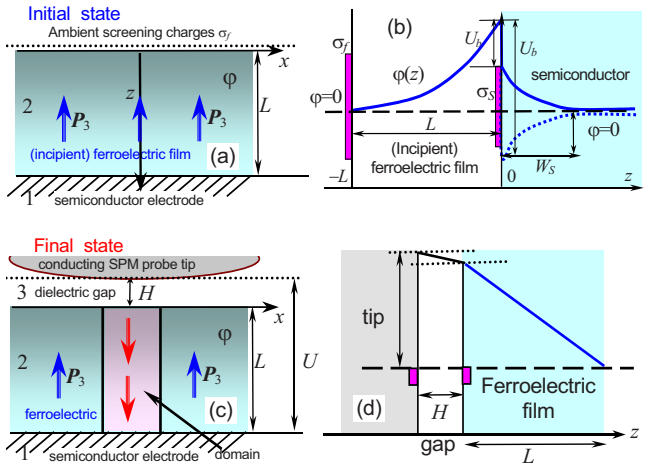

FIG. 1. (Color online) (a) The initial state of the considered heterostructure: semiconductor/(incipient or proper) ferroelectric-dielectric film of thickness L. P_3 is the ferroelectric polarization. (b) Sketch of the electrostatic potential distribution: φ is the electrostatic potential, U_b is the contact potential difference on ferroelectric-semiconductor interface, W_S is the electric field penetration depth into the semiconductor, i.e., the thickness of the space-charge depletion layer (shown by dashed and solid lines for different charge signs. Prolate rectangles show the interface (σ_f) and surface (σ_S) charges. (c) The final state of the ferroelectric film is the local polarization reversal caused by the biased SPM probe. (d) During the tip-induced polarization reversal an ultrathin dielectric gap H between the tip electrode and the ferroelectric surface could exist. Squares denote the screening surface charges σ_f and the opposite charge accommodated at the tip surface.

ferroelectric film of thickness L. We will consider the two cases of the proper and incipient ferroelectric films, both either a wide-gap semiconductor or a dielectric (i.e., semiconducting properties of ferroelectric are neglected). In the initial state, the external bias is absent and the free ferroelectric surface $z=-L$ is completely screened by the ambient sluggish charges [Fig. 1(a)]. Then inhomogeneous external bias $U(x,y)$ is applied to the tip electrode. The bias increase may cause local polarization reversal below the tip that finally results into cylindrical domain formation in thin ferroelectric film [see the final state in Fig. 1(c)]. Note that while we consider the tip-induced polarization switching, the obtained solutions are applicable for capacitor geometry in the limit of uniform potential.

The contact potential difference U_b at the interface $z=0$ originates from the band mismatch between ferroelectric and semiconductor, the interface bonding effect, and interfacial polarity [Fig. 1(b)]. The band bending in the semiconductor leads to the depleted charged layers of thickness W_S with space charge ρ_S.

The screening interface charge σ_S could originate at $z=0$ self-consistently in the case of the bad screening from the semiconductor side (i.e., for thick depletion layer created by the minor-type carriers). The nonideal screening that causes the strong depolarization field controls the self-consistent mechanism. The field decreases the polarization inside the ferroelectric film and increases the free energy of the system since depolarization field energy is always positive. As a result, the strong field effect may lead to the bend bending at $z=0$ and appearance of charge states at the interface. The interface charges σ_S of appropriate sign provide effective screening of the spontaneous polarization, make it more homogeneous and thus decrease the depolarization field, which in turn self-consistently decreases the system free energy. The density of the interface charge σ_S depends on energetic position of chemical potential μ at the surface that modifies the Shottky barrier. The potential μ is manly determined by the interface layers with the energy density N_S (per unit energy) of quasicontinuous surface states and Fermi level E_F at the neutral surface.[15–17]

We assume that in the initial state the sluggish surface charges σ_f completely screen the electric displacement outside the film, i.e., $\sigma_f(x,y,-L)=-D_3(x,y,-L)$, $\varphi(x,y,-L)=0$, and $D_3(z<-L)=0$. This behavior is analyzed in Sec. III.

In contrast, recharging of the surface charges σ_f should appear during the polarization reversal due to the ambient charges accommodation, displacement current, and tunneling effects as explained below. The ultrathin dielectric gap of thickness H models the resistive properties of the sluggish surface charges σ_f, contamination or dead layer, as well as physical gap between the tip and the ferroelectric film surface. Due to the displacement current corresponding to the polarization reversal, free charges $-\sigma_f$ are instantly accommodated at the conducting SPM tip surface. Then the electron's tunneling across the gap would result in the gradual neutralization of the uncompensated charges $\sigma_{uncop}(x,y,t)=\sigma_f(x,y,-L,t)+D_3(x,y,-L,t)$ and thus to the self-consistent lowering of the potential barrier between the SPM tip and the ferroelectric film surface $z=-L$. The process is dynamic, resulting into the complex temporal dependence of the total electric current consisting of the "fast" polarization-reversal contribution and the relatively "slow" tunneling current estimated in the end of the Sec. IV. The tunneling current stops only when the full neutralization of the uncompensated charges is reached.

Without loss of generality one can assume that the equilibrium domain structure is almost cylindrical for the case of complete local polarization reversal in thin ferroelectric film. The assumptions significantly simplify the problem considered in the Sec. IV and allow developing the analytical description for the domain formation.

Hereinafter we assume that the time of external field changing is small enough for the validity of the quasistatic approximation $rot\mathbf{E}\approx 0$. Maxwell's equations for the quasistatic electric field $\mathbf{E}=-\nabla\varphi$ and displacement $\mathbf{D}$ inside semiconductors have the form

$$\mathrm{div}\,\mathbf{D}=\mathrm{div}(\varepsilon_0\mathbf{E}+\mathbf{P})=\rho(\varphi). \tag{1}$$

Here the electrostatic potential $\varphi(x,y,z)$ is determined by external bias as well as by contact and surface effects. The potential is interdependent with the free carrier density $\rho(\varphi)$ determined by the concentration of holes in the valence band, electrons in the conduction band, and acceptors and donors at their respective levels in the band gap.[16]

The ferroelectric film that occupies the region $-L<z<0$ is transversally isotropic, i.e., permittivity $\varepsilon_{11}=\varepsilon_{22}$ at zero electric field. We further assume that the dependence of in-

plane polarization components on $E_{1,2}$ can be linearized as $P_{1,2} \approx \varepsilon_0(\varepsilon_{11}-1)E_{1,2}$ (ε_0 is the universal dielectric constant) while the polarization component P_3 nonlinearly depends on external field. Thus corresponding polarization vector acquires the form: $\mathbf{P}(\mathbf{r})=[\varepsilon_0(\varepsilon_{11}-1)E_1, \varepsilon_0(\varepsilon_{11}-1)E_2, P_3(\mathbf{E},\mathbf{r}) + \varepsilon_0(\varepsilon_{33}^b-1)E_3]$.[18]

Within the framework of the LGD theory, quasiequilibrium polarization distribution $P_3(\mathrm{x},\mathrm{y},z)$ in the ferroelectric film with the spatial dispersion should be found from the Euler-Lagrange boundary problem

$$\begin{cases} \Gamma\dfrac{\partial}{\partial t}P_3 + \alpha P_3 + \beta P_3^3 + \gamma P_3^5 - g\left(\Delta_\perp + \dfrac{\partial^2}{\partial z^2}\right)P_3 = -\dfrac{\partial \phi}{\partial z}, \\ \left(P_3 + \lambda_1\dfrac{\partial P_3}{\partial z}\right)\Bigg|_{z=0} = -P_b, \left(P_3 - \lambda_2\dfrac{\partial P_3}{\partial z}\right)\Bigg|_{z=-L} = 0. \end{cases} \tag{2}$$

Hereinafter we introduced a transverse Laplace operator $\Delta_\perp = \frac{\partial^2}{\partial x^2} + \frac{\partial^2}{\partial y^2}$. The initial condition $P_3(x,y,z,t=0)$ corresponds to the single-domain state. Kinetic coefficient $\Gamma > 0$.

The temperature-dependent coefficient α is positive for incipient ferroelectric and proper ferroelectrics in paraelectric phase, while $\alpha < 0$ for proper ferroelectrics in ferroelectric phase, $\beta > 0$ for the second-order ferroelectrics mainly considered hereinafter, gradient coefficient $g > 0$. Extrapolation lengths $\lambda_{1,2}$ originate from the surface-energy coefficients in the LGD-free energy.

Inhomogeneity P_b describes the effect of the interface polarization stemming from the interface bonding effect and associated interface dipole.[19,20] More generally, the translation symmetry breaking inevitably present in the vicinity of the any interface will give rise to inhomogeneity in the boundary conditions in Eq. (2).[21,22]

Eqs. (1) and (2) yield the coupled system

$$\left(\frac{\partial^2\varphi}{\partial z^2} + \Delta_\perp\varphi\right) = 0, \quad -H-L < z < -L,$$

$$\varepsilon_{33}^b\frac{\partial^2\varphi}{\partial z^2} + \varepsilon_{11}\Delta_\perp\varphi = \frac{1}{\varepsilon_0}\left[\frac{\partial P_3}{\partial z} - \rho_f(\varphi)\right], \quad -L < z < 0,$$

$$\varepsilon_0\varepsilon_S\left(\frac{\partial^2\varphi}{\partial z^2} + \Delta_\perp\varphi\right) = -\rho_S(\varphi), \quad z > 0. \tag{3}$$

The background dielectric permittivity of (incipient) ferroelectric ε_{33}^b (typically $\varepsilon_{33} \gg \varepsilon_{33}^b$); ε_S is the semiconductor (bare) lattice permittivity.

Equations (3) are supplemented with the boundary conditions at $z=-L-H$, $z=-L$, $z=0$, and $z=+\infty$, namely,

$$\varphi(x,y,-L-H) = U_e(x,y),$$

$$\varphi(x,y,-L+0) = \varphi(x,y,-L-0),$$

$$\varphi(x,y,z\to\infty) = 0, \tag{4a}$$

$$\varphi(x,y,+0) - \varphi(x,y,-0) = U_b, \tag{4b}$$

$$\varepsilon_0\varepsilon_{33}^b\frac{\partial\varphi(x,y,-0)}{\partial z} - P_3(x,y,-0) - \varepsilon_S\varepsilon_0\frac{\partial\varphi(x,y,+0)}{\partial z} = \sigma_S(x,y), \tag{4c}$$

$$-\varepsilon_0\varepsilon_{33}^b\frac{\partial\varphi(x,y,-L+0)}{\partial z} + P_3(x,y,-L+0) + \varepsilon_{33}^g\varepsilon_0\frac{\partial\varphi(x,y,-L-0)}{\partial z} = \sigma_f(x,y), \tag{4d}$$

where U_b is the contact potential difference at the dielectric-semiconductor interface. ε_{33}^g is the dielectric constant of the dielectric gap between the tip and ferroelectric surface. The potential distribution $U_e(x,y)$ produced by the SPM tip is assumed to be almost constant in the surface spatial region much larger then the film thickness.

III. SOLUTION FOR POLARIZATION, ELECTRIC POTENTIAL, AND FIELD AND SPACE CHARGE DISTRIBUTIONS

A. Analytical solutions for the one-dimensional case

Here we calculate the potential and polarization distribution in the initial ground state in the one-dimensional (1D) case U_e=const. that corresponds to the plane electrodes. The case is realized in paraelectric or incipient ferroelectric film as well as in the monodomain state of the proper ferroelectric thin film.

The space-charge density inside the doped p-type (or n-type) semi-infinite semiconductor has the form

$$\rho_S(\varphi) = q[p(\varphi) + N_d^+(\varphi) - n(\varphi) - N_a^-(\varphi)],$$

$$p(\varphi) = N_p^0 \cdot F\left(\frac{E_F - E_V + q\varphi}{k_BT}\right),$$

$$N_d^+(\varphi) = N_d \cdot F\left(\frac{E_F - E_d + q\varphi}{k_BT}\right),$$

$$n(\varphi) = N_e^0 F\left(\frac{E_C - E_F - q\varphi}{k_BT}\right), \quad N_a^-(\varphi) = N_a F\left(\frac{E_a - E_F - q\varphi}{k_BT}\right), \tag{5a}$$

where $F(\theta)=[\exp(\theta)+1]^{-1}$ is the Fermi-Dirac distribution function, q is the absolute value of the carrier elementary charge. E_F, E_V, E_C, E_d, and E_a are the energies of Fermi level, valence band, conductance band, and donor and acceptor levels in the quasineutral region of the semiconductor correspondingly. Since $\rho_S(\varphi)\to 0$ in the quasineutral region of the semiconductor, where $\varphi\to 0$, the identity $p(0) + N_d^+(0) - n(0) - N_a^-(0) = 0$ should be valid. The identity along with typical assumption $N_d^+ \approx$ const, $N_a^- \approx$ const. and Boltzman approximation for electrons $E_C - E_F - q\varphi \gg k_BT$ or holes $E_F - E_V + q\varphi \gg k_BT$ lead to expressions $\rho_S \approx qp_S^0[\exp(-\frac{q\varphi}{k_BT}) - 1]$ or $\rho_S \approx -qn_S^0[\exp(\frac{q\varphi}{k_BT}) - 1]$ correspondingly, where p_S^0 and n_S^0 are equilibrium concentrations of holes and electrons in the quasineutral region of the semiconductor.[23]

Then in depletion layer (or abrupt junction) approximation the space charge density near the interface of the strongly doped p-type (or n-type) semi-infinite semiconductor has the form

$$\rho_S(\varphi) \approx \begin{cases} \rho_S^0 & 0 < |z| < W_S \\ 0 & |z| > W_S. \end{cases} \tag{5b}$$

Hereinafter the choice of the charge density $\rho_S^0 = qp_S^0$ and depth $W_S = W_{Sp}$ (or $\rho_S^0 = -qn_S^0$ and $W_S = W_{Sn}$) is determined by the sign of potential (i.e., by the sign of charge in depletion layer). More rigorously, for the definite type of carriers the thicknesses of the depletion layers W_S (i.e., the field penetration depths) should be determined self-consistently from the exact solution of the system, Eqs. (3), (4a)–(4d), and (5).

The ferroelectric film is regarded as a wide-gap proper semiconductor or almost dielectric so its space-charge density is negligibly small: $\rho_f(\varphi) \approx 0$ at $-L < z < 0$. The nonzero 1D solution of Eqs. (3) with respect to the boundary conditions in Eqs. (4a), (4c), and (4d) is

$$\varphi(z) \approx \begin{cases} -\dfrac{\rho_S^0}{2\varepsilon_0\varepsilon_S}(W_S - z)^2\theta(W_S - z), & z > 0 \\ \displaystyle\int_{-L}^{z} \frac{P_3(\tilde{z})}{\varepsilon_0\varepsilon_{33}^b} d\tilde{z} - (L+z)\left(\frac{\rho_S^0 W_S - \sigma_S}{\varepsilon_0\varepsilon_{33}^b}\right) + U_e + \frac{H}{\varepsilon_0\varepsilon_{33}^g}(\sigma_S + \sigma_f - \rho_S^0 W_S), & -L \le z < 0 \\ U_e + \dfrac{H+L+z}{\varepsilon_0\varepsilon_{33}^g}(\sigma_S + \sigma_f - \rho_S^0 W_S), & -L-H \le z < -L. \end{cases} \tag{6}$$

Here $\theta(z)$ is the step function. So the semiconductor potential and space charge are distributed in the layer $0 < z < W_S$ and zero outside. Approximate expressions in Eq. (6) for the potential φ correspond to parabolic approximation valid in the depletion/accumulation limit, at that $W_{Sn} \ll W_{Sp}$ or $W_{Sn} \gg W_{Sp}$ depending of the main carriers n or p type. Note, that in the accumulation regime the interface charge σ_S is localized in the thin depletion layer of several nm (for oxide electrodes) thickness W_S that is occupied by the main-type carriers. The opposite case of charged layers created by the minor-type carriers, which can appear during the polarization reversal, could lead the strong band bending and accommodation of σ_S.

From Eq. (6) we derived the electric field E_3 and electrical displacement D_3 distributions in the parabolic approximation

$$E_3(z) \approx -\frac{\sigma_S + \sigma_f - \rho_S^0 W_S}{\varepsilon_0\varepsilon_{33}^g},$$

$$D_3(z) = -\sigma_S - \sigma_f + \rho_S^0 W_S,$$

at

$$-L-H \le z < -L,$$

$$E_3(z) \approx -\frac{P_3(z)}{\varepsilon_0\varepsilon_{33}^b} + \frac{\rho_S^0 W_S - \sigma_S}{\varepsilon_0\varepsilon_{33}^b}, \quad D_3(z) = \rho_S^0 W_S - \sigma_S,$$

at

$$-L < z < 0,$$

$$E_3(z) \approx \frac{\rho_S^0}{\varepsilon_0\varepsilon_S}(z - W_S)\theta(W_S - z), \tag{7}$$

$$D_3(z) = \rho_S^0(z - W_S)\theta(W_S - z),$$

at $z > 0$. Note, that due to the ambient humidity and tunneling effects the free sluggish screening charge $\sigma_f(t)$ with characteristic relaxation time τ_S should originate at the another interface $z = -L$. Under the condition $\sigma_f(t \gg \tau_S) \to -\sigma_S + \rho_S^0 W_S$ the electric field in the gap tends to zero and any current stops self-consistently when the system reaches the final equilibrium state. The relaxation time τ_S may be relatively high or relatively small in comparison with the polarization relaxation time $\tau_P \sim \Gamma/|\alpha|$ that rules the time scale in Eq. (2). In order to obtain analytical expressions, three limiting cases are considered below: (a) quasiequilibrium polarization $P_3(z)$ relaxation for the uncompensated charge σ_f, which is possible at the times $\tau_P \ll t \ll \tau_S$ and condition $\tau_S \gg \tau_P$ (adiabatic approximation); (b) the final state $\sigma_f = -\sigma_S + \rho_S^0 W_S$ reached at the times $t \gg \tau_S$ and $t \gg \tau_P$; and (c) relaxed polarization at $t \gg \tau_P$ and $H = 0$ (no gap and no tunneling current).

Allowing for Eqs. (6) and (7) the quasiequilibrium polarization distribution $P_3(z, t \gg \tau_P)$ was found from the static Euler-Lagrange boundary problem in Eq. (2) as described in Appendix A. At the times $t \gg \tau_P$ the polarization distribution acquires the form

$$P_3(z) = \frac{\varepsilon_S - 1}{\varepsilon_S}\rho_S^0(z - W_S) \cdot \theta(W_S - z), \quad z \ge 0, \tag{8a}$$

$$P_3(z) = \frac{2\varepsilon_0\varepsilon_{33}^b\langle P_3\rangle^3(\beta + 2\gamma\langle P_3\rangle^2) + \rho_S^0 W_S - \sigma_S}{\varepsilon_0\varepsilon_{33}^b(\alpha + 3\beta\langle P_3\rangle^2 + 5\gamma\langle P_3\rangle^4) + 1} f(z,L) - P_b b(z,L), \quad -L < z \le 0. \tag{8b}$$

Parameter $\langle P_3\rangle$ in Eq. (8b) is the polarization averaged over the film depth: $\langle P_3\rangle \equiv \frac{1}{L}\int_{-L}^{0} P_3(\tilde{z})d\tilde{z}$. The polarization spatial distribution is governed by the functions f and b

$$f(z,L) = 1 - \xi\frac{\lambda_2 \cosh[(L+z)/\xi] + \lambda_1 \cosh(z/\xi) + \xi\{\sinh[(L+z)/\xi] - \sinh(z/\xi)\}}{(\xi^2+\lambda_1\lambda_2)\sinh(L/\xi) + \xi(\lambda_1+\lambda_2)\cosh(L/\xi)}, \tag{9a}$$

$$b(z,L) = \frac{\xi\lambda_2 \cosh[(L+z)/\xi] + \xi^2 \sinh[(L+z)/\xi]}{(\xi^2+\lambda_1\lambda_2)\sinh(L/\xi) + \xi(\lambda_1+\lambda_2)\cosh(L/\xi)}. \tag{9b}$$

Characteristic length $\xi \approx \sqrt{\varepsilon_0\varepsilon_{33}^b g}$.

The average polarization $\langle P_3\rangle$ and depths $W_{Sn,p}$ should be determined self-consistently from the spatial averaging of Eq. (8b) and the boundary conditions in Eq. (4b). After elementary transformations we obtained the system of two coupled algebraic equations

$$\begin{cases} \langle P_3\rangle = \rho_S^0 W_S - \sigma_S + \dfrac{\varepsilon_{33}^b\rho_S^0}{2L\varepsilon_S}W_S^2 - \dfrac{\varepsilon_0\varepsilon_{33}^b}{L}\left[U_b + U_e + \dfrac{H}{\varepsilon_0\varepsilon_{33}^g}(\sigma_S + \sigma_f - \rho_S^0 W_S)\right] \\ \left(\alpha + \dfrac{1}{\varepsilon_0\varepsilon_{33}^b}\right)\langle P_3\rangle + \beta\langle P_3\rangle^3(3-2\langle f\rangle) + \gamma\langle P_3\rangle^5(5-4\langle f\rangle) = \left(\dfrac{\rho_S^0 W_S - \sigma_S}{\varepsilon_0\varepsilon_{33}^b}\right)\langle f\rangle - \dfrac{P_b}{\varepsilon_0\varepsilon_{33}^b}\langle b\rangle, \end{cases} \tag{10}$$

where the average values $\langle f\rangle \approx 1 - \frac{\xi^2(2\xi+\lambda_1+\lambda_2)}{L[\xi(\lambda_1+\lambda_2)+\xi^2+\lambda_1\lambda_2]}$ and $\langle b\rangle \approx \frac{\xi^2}{L(\xi+\lambda_1)}$.

For $H \neq 0$ one should put the surface-charge density $\sigma_f = \rho_S^0 W_S - \sigma_S$ in the final (or ground) state, when the electric current and field are absent inside the gap [see Eq. (7)]. Thus we should put $\sigma_f = -\sigma_S + \rho_S^0 W_S$ for the stable or metastable states calculations from Eqs. (6), (7), (8a), (8b), (9a), (9b), and (10) in the Secs. III C and IV, which is mathematically equivalent to the condition $H=0$.

During the system relaxation to the equilibrium the density σ_f may vary self-consistently until reaches the value $(\rho_S^0 W_S - \sigma_S)$ at times $t \gg \tau_S$. To account for the possible changes in σ_f in the "adiabatic approximation" $\tau_S \gg \tau_P$, below we introduce the *dimensionless degree of surface screening* μ, namely, $\sigma_f = \mu(\rho_S^0 W_S - \sigma_S)$, at that $0 < \mu < 1$ at times $t < \tau_S$ and $\mu \to 1$ at times $t \gg \tau_S$.

Eqs. (8) and (9) and transcendental relations in Eq. (10) are valid for both the first- and the second-order ferroelectric films with arbitrary thickness. Expressions (8a), (8b), (9a), (9b), and (10) will be used in the Secs. III C and III D while below we derive approximate evident expressions for the second-order ferroelectrics.

B. Stability of the "up" and "down" polarization states for the second-order ferroelectrics

In particular case of the narrow-gap semiconductor and thick-enough film of the second-order ferroelectrics the strong inequality $W_S \ll L$ is valid and all terms proportional to γ could be neglected for qualitative description since $\beta > 0$. These assumptions lead to the linear approximation in Eq. (10), namely, $\langle P_3\rangle \approx (\rho_S^0 W_S - \sigma_S)[1 + \frac{\varepsilon_{33}^b H}{\varepsilon_{33}^g L}(1-\mu)] - \frac{\varepsilon_0\varepsilon_{33}^b}{L}(U_b + U_e)$, which gives the cubic equation for the average polarization

$$\left\{\alpha + \frac{1}{\varepsilon_0\varepsilon_{33}^b}\left[1 - \frac{\varepsilon_{33}^g L\langle f\rangle}{\varepsilon_{33}^g L + \varepsilon_{33}^b(1-\mu)H}\right]\right\} \times \langle P_3\rangle + \beta\langle P_3\rangle^3(3-2\langle f\rangle) = E_b^f(L,H) + E_e^f(L,H). \tag{11a}$$

where the built-in electric field $E_b^f(L,H)$ and external field $E_e^f(L,H)$ are introduced as

$$E_b^f(L,H) = \frac{\varepsilon_{33}^g\langle f\rangle U_b}{\varepsilon_{33}^g L + \varepsilon_{33}^b(1-\mu)H} - \frac{P_b}{\varepsilon_0\varepsilon_{33}^b}\langle b\rangle, \tag{11b}$$

$$E_e^f(L,H) = \frac{\varepsilon_{33}^g\langle f\rangle U_e}{\varepsilon_{33}^g L + \varepsilon_{33}^b(1-\mu)H}. \tag{11c}$$

Note that Eq. (11a) this is equivalent to the equation for ferroelectric polarization hysteresis loop in the uniform electric field while the built-in field $E_b^f(L,H)$ determines the horizontal imprint of the loop. Thus for the case considered by Eqs. (11) the symmetric intrinsic coercive fields $E_c^b = \pm\frac{2}{3\sqrt{3}}\sqrt{-\frac{\alpha^3}{\beta}}$ of a bulk material[24] become asymmetric and have the form.

$$E_c^{\pm} = -E_b^f(L,H) \pm \frac{2}{3\sqrt{3}}\sqrt{-\frac{1}{\beta(3-2\langle f\rangle)}\left\{\alpha(T)+\frac{1}{\varepsilon_0\varepsilon_{33}^b}\left[1-\frac{\varepsilon_{33}^g L\langle f\rangle}{\varepsilon_{33}^g L+\varepsilon_{33}^b(1-\mu)H}\right]\right\}^3}. \tag{12}$$

Renormalization of the coefficient α in Eq. (11), i.e., the term $\frac{1}{\varepsilon_0\varepsilon_{33}^b}[1-\frac{\varepsilon_{33}^g L\langle f\rangle}{\varepsilon_{33}^g L+\varepsilon_{33}^b(1-\mu)H}]$, quantitatively reflects the "extrinsic contribution" [factor $0<\frac{\varepsilon_{33}^g L}{\varepsilon_{33}^g L+\varepsilon_{33}^b(1-\mu)H}<1$] originated from the depolarization field produced by the finite gap H and the "intrinsic contribution" (factor $0<\langle f\rangle\leq 1$) originated from the finite extrapolation lengths $\lambda_i<\infty$ and intrinsic polarization gradient ($\langle f\rangle=1$ for either $g=0$ or both $\lambda_i=\infty$). Thus Eq. (11) allows rigorous estimations of both extrinsic and intrinsic contributions into the renormalization of the transition temperature into paraelectric phase (compare the result for the case $\mu=0$ with Ref. 25).

For proper ferroelectrics the coefficient $\alpha(T)=\alpha_T(T-T_c^*)$, where T is the absolute temperature. T_c^* is the Curie temperature renormalized by the epitaxial misfit strain $u_m=(a/c)-1$. The strain originated from the thin film (a) and semiconductor (c) lattice constants mismatch (see Ref. 26 for details).

For the cube-on-cube epitaxy of perovskites and considered out-of-plane polarization geometry $T_c^*=T_c+\frac{u_m^*}{\alpha_T}\frac{4Q_{12}}{s_{11}+s_{12}}$, where s_{ijkl} is the compliances tensor positively defined, Q_{ijkl} stands for the electrostriction strain tensor, u_m^* is the *effective* misfit strain, at that $u_m^*(L)\approx u_m$, $L\leq h_d$ and $u_m^*(L)\approx u_m h_d/L$, $L>h_d$ (h_d is the critical thickness of dislocations appearance).[22] For thin films the coefficient β is also renormalized by the misfit strain as:[26] $\beta=\beta_b+\frac{4Q_{12}^2}{s_{11}+s_{12}}$ (β_b is the bulk value). However for the opposite case $L\gg h_d$ it should be $\beta\to\beta_b$ and we estimated the asymptotic law as $\beta\approx\beta_b+\frac{4Q_{12}^2}{s_{11}+s_{12}}\frac{h_d^2}{L^2}$.

Actually, it is well-known fact that misfit dislocations originate in epitaxial films when their thickness is more than the critical thickness of dislocations appearance h_d.[27] The thickness decreases with the interface misfit strain u_m increase. In accordance with the Matthews-Blakeslee theory and Speck and Pompe model for perovskites, $h_d\approx\frac{b}{u_m}\frac{\sqrt{2}\ln(4h_d/b)}{8\pi(1+\nu)}\sim u_m^{-1}$ in the wide range of u_m, which is in good agreement with experiments and ($b\sim a$ is the Burgers vector of dislocation, $\nu\sim 0.3$ is the Poisson's ratio). For typical misfit strains $|u_m|\sim 10^{-2}$ the thickness $h_d\sim 10-0.5$ nm, i.e., it is not more than several tens of lattice constants.[27] Estimations show that the strain renormalization of α and β is important for ultrathin ferroelectric films with thickness L smaller than h_d and becomes negligibly small for films with $L\gg h_d$. (see the Table II in Sec. III C).

Hence, the critical thickness (as well as the critical temperature) of the size-induced transition of the ferroelectric film into paraelectric phase can be found from the condition $\alpha+\frac{1}{\varepsilon_0\varepsilon_{33}^b}[1-\frac{\varepsilon_{33}^g L\langle f\rangle}{\varepsilon_{33}^g L+\varepsilon_{33}^b(1-\mu)H}]=0$ as

$$L_{cr}(T)\approx -\frac{1}{\varepsilon_0\alpha(T)}\left\{\frac{\xi^2(2\xi+\lambda_1+\lambda_2)}{\varepsilon_{33}^b[\xi(\lambda_1+\lambda_2)+\xi^2+\lambda_1\lambda_2]}+\frac{(1-\mu)H}{\varepsilon_{33}^g}\right\} \tag{13}$$

$$T_{cr}(L)\approx T_c^*-\frac{1}{\alpha_T\varepsilon_0\varepsilon_{33}^b}\left(1-\frac{\varepsilon_{33}^g L}{\varepsilon_{33}^g L+\varepsilon_{33}^b(1-\mu)H}\times\left\{1-\frac{\xi^2(2\xi+\lambda_1+\lambda_2)}{L[\xi(\lambda_1+\lambda_2)+\xi^2+\lambda_1\lambda_2]}\right\}\right) \tag{14}$$

For unstrained incipient ferroelectric film the coefficient $\alpha(T)$ is positive up to zero temperatures and typically is given by Barret's formula, $\alpha=\alpha_T[\frac{T_q}{2}\coth(\frac{T_q}{2T})-T_c^*]$. Thus the critical temperature (as well as the critical thickness) does not exist for $T_c^*<0$ since the film remained paraelectric up to zero Kelvin. However for the strained film T_c^* may become positive, indicative of the transition to the ferroelectric state.[28]

For particular case $H=0$ (gap is absent) the build-in field E_b^f is inversely proportional to the film thickness, $E_b^f(L,0)\approx B/L$, while its value depends on the built-in polarization P_b, surface charge σ_f, and contact potential difference U_b [see Eq. (11b) and the dashed almost straight line in Fig. 2(a)]. The build-in field E_b^f leads to the vertical asymmetry and horizontal imprint of the polarization hysteresis loops in ferroelectric films of thickness more than critical $L>L_{cr}(T)$ [see regions 2 and 3 in Figs. 2(a) and 2(b)]. Field-induced

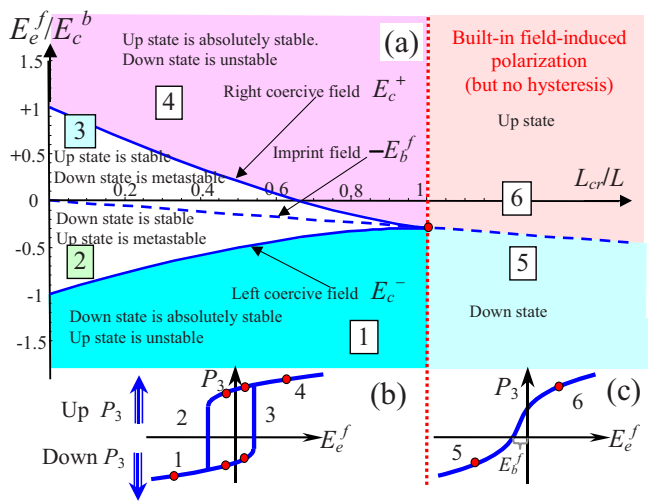

FIG. 2. (Color online) (a) Diagram in coordinates "field-inverse thickness," $\{\frac{E_e^f}{E_c^b},\frac{L_{cr}}{L}\}$ that shows the stability of the up ($\langle P_3\rangle>0$) and down ($\langle P_3\rangle<0$) polarization states in a ferroelectric film. Dashed curve is the thickness dependence of the built-in field $-E_b^f(L)$ calculated from Eq. (11b); solid curves are thickness dependences of right and left coercive fields $E_c^{\pm}(L)$ calculated from Eqs. (11b) and (12) at $H=0$, fixed temperature and extrapolation lengths. E_c^b is the absolute value of the bulk coercive field, L_{cr} is the film critical thickness given by Eq. (13). [(b) and (c)] Hysteresis loops schematics in a ferroelectric phase (b) and field-induced polarized state (c).

polarized state appears at film thickness less than the critical one $L<L_{cr}(T)$ [see regions 5 and 6 in Figs. 2(a) and 2(c)].

For typical ferroelectric material parameters approximate expressions for the right and left coercive biases are $E_c^{\pm}(L,0,T)\approx-(B/L)\pm E_c^b(T)\sqrt{[1-L_{cr}(T)/L]^3}$ [see Eq. (12)]. Thus solid curves in Fig. 2(a) look like an asymmetric "bird beak" with the tip $E_c^{\pm}(L=L_{cr})\approx-(B/L_{cr})$ and asymptotes $E_c^{\pm}(L\gg L_{cr})\rightarrow\pm E_c^b(T)$. The built-in field sign and thickness dependence determine the beak ⟨⟨up⟩⟩ or ⟨⟨down⟩⟩ asymmetry and shape correspondingly.

Note, that there may be two possible solutions corresponding to the polarization up and down. Region 4 in Fig. 2(a) corresponds to the stable "up" polarization states ($\langle P_3\rangle>0$), metastable states are absent here. The situation is vise versa in the region 1. Region 6 corresponds to the up polarization. The situation is vise versa in the region 5. Hysteresis loops are absent in the thickness regions 5 and 6, since at thicknesses $L<L_{cr}$ the loops never exist, here renormalized coefficient α becomes positive and coercive bias given by Eq. (12) is complex value.

Bistability of polarization states exists only in the regions 2 and 3. Up states are absolutely stable in the region 3 while the "down" state is metastable here. The situation is vise versa in the region 2. The depletion lengths $W_{Sn,p}$ are at least several times different for to the up and down polarization states. In the next sections we will show how the presence of build-in field E_b^f smear the size-induced phase transition and induces polarization in the incipient ferroelectric films.

C. Calculations of the stable ground state for typical heterostructures (1D case, $U_e=0$)

Here we calculate the potential and polarization distribution in the absolutely stable ground state, metastable states will be discussed in the next section. First, we derive the field structure for the case when the external bias is absent ($U_e=0$). This one-dimensional case is realized in paraelectric or incipient ferroelectric film as well as in the monodomain state of the proper ferroelectric thin film. We assume that the surface charge σ_f localized at $z=-L$ should provide the full screening of the spontaneous polarization outside the film and minimize the depolarization field energy, i.e., they acts as a perfect electrode and thus provide $D_3(z=-L+0)=\sigma_f$ and $D_3(z<-L-0)=E_3(z<-L-0)=0$. Thus we should put $\sigma_f=-\sigma_S+\rho_S^0W_S$ for the stable or metastable states calculations from Eqs. (6), (7), (8a), (8b), (9a), (9b), and (10), which is mathematically equivalent to the condition $H=0$.

From relations (10) one can determine the thickness dependence of penetration depths $W_{Sp,n}$ and polarization $\langle P_3\rangle$ for different extrapolation lengths, since the quantities U_b, n_S^0, p_S^0 ε_S, and ε_{33}^b can be regarded as known material parameters. LGD-expansion coefficients α, β, and the gradient coefficient g are tabulated for the majority of proper and incipient ferroelectrics.

Material parameters used in the calculations of the heterostructures $SrTiO_3/(La,Sr)MnO_3$ (STO/LSMO) and $BiFeO_3/(La,Sr)MnO_3$ (BFO/LSMO) polar properties are listed in the Table I. Estimations show that the renormalization of α and β by misfit strain u_m for LSMO/STO and LSMO/BFO heterostructures is important for thin films with thickness smaller than the critical thickness of misfit dislocations 2–10 nm and becomes negligibly small for ferroelectric films with thickness more than several dozens of nm (see Table II).

Extrapolation lengths λ_i and interface charge σ_S values are not listed in the Table I since they strongly depend on the interfacial states. Extrapolation length values could be extracted from the polarization distribution in ferroelectric nanosystems (films, wires, etc.) obtained either experimentally[42,43] or determined by the first-principles calculations.[19,20] Extremely small and extremely high values of extrapolation lengths describe the two limiting cases of the surface-energy contribution to the total free energy. Extremely small values of λ_i correspond to complete suppression of the polarization on the surface while extremely large ones—to the absence of the surface energy dependence on polarization (so-called natural boundary conditions). Allowing for the remark below we consider two limiting cases of the small and high values of extrapolation lengths.

The polar interface may produce a positive ionic charge leading to displacements in LSMO. Figure 3 shows z distributions of the electric polarization in the heterostructure "ferroelectric $BiFeO_3$ film—half-metal $LaSrMnO_3$" (BFO/LSMO) for different values of interface polarization P_b and interface charge σ_S. It is seen that the polarization distribution near z=0 and its asymmetry are the main effects of the interface polarization while the interface charge creates the homogeneous electric field inside the ferroelectric film. That is why the effect of P_b on the polarization distribution is much weaker than the effect of σ_S. Below we consider the case $P_b=0$.

Figure 4 shows z dependence of the electric polarization, potential, and field and bulk charge density in the heterostructure of BFO/LSMO for different interface polarization P_b, fixed extrapolation length, and interface charge σ_S. Note that extrapolation length increase as well as the film thickness increase lead to the decrease in P_b effect on the film polar properties.

Figures 5 and 6 show the spatial distribution of electric polarization, potential, and field and bulk charge density in the heterostructure BFO/LSMO for zero interface charge $\sigma_S=0$. When generating the plots in Figs. 5 we use small λ_i. Plots in Figs. 6 correspond to high-enough λ_i values. As anticipated the polarization distribution is almost homogeneous for the high extrapolation length. For a small extrapolation length the polarization profile is more inhomogeneous.

Figures 7 and 8 illustrate z distributions of the electric polarization, potential, and field and bulk charge density in the heterostructure "incipient $SrTiO_3$ film—half-metal $LaSrMnO_3$" (STO/LSMO) for zero interface charge $\sigma_S=0$. When generating the plots in Figs. 7 we use small λ_i. Plots in Figs. 8 correspond to high enough λ_i values. The resulting built-in field $E_b^f\sim(\frac{U_b}{L}\langle f\rangle-\frac{P_b}{\varepsilon_0\varepsilon_{33}^b}\langle b\rangle)$ [see Eq. (11b)] induces the electric polarization in the incipient ferroelectric films.

The distributions shown in Figs. 7 and 8 correspond to the stable ground state of the heterostructure incipient ferroelectric STO/LSMO without interface charge ($\sigma_S=0$), i.e., when the free carriers are abundant in LSMO and there is no need

TABLE I. Parameters of the bulk materials.

Material	Band gap (eV)	Carries concentration (cm^{-3})	Background permittivity, LGD-expansion coefficients for ferroelectrics, electrostriction, and elastic constants
$LaSrMnO_3$ (LSMO) half-metal	1 p type (Refs. 29 and 30)	1.83×10^{22} (Ref. 31)1.65×10^{21} (Ref. 32)($La_{0.7}Sr_{0.3}MnO_3$)	$\varepsilon_S=30$ (Ref. 33) effective lattice constant $a=3.876$ Å Nonferroelectric
$BiFeO_3$ (BFO) ferroelectric	3	Wide band-gap semiconductor	${\varepsilon_{33}}^b=9.0$ [a]) (Ref. 34) $a=3.965$ Å, effective lattice constant $a_{hex}=5.58$ Å $\alpha_T=2.3\times10^5$ m/(F K), $T_c=1098-1103$ K, $T=300$ K, $\beta_b=-2.44\times10^9$ $m^5/(C^2F)$, $\gamma=1.56\times10^{10}$ $m^9/(C^4F)$ [extracted from data on static permittivity from (Ref. 34)], $P_S=0.8$ C/m^2 (Refs. 35 and 36) $g=10^{-8}-10^{-9}$ m^3/F [below we used the value 1.3×10^{-8} m^3/F extracted from STEM data (Ref. 37)] $Q_{11}=0.032$ m^4/C^2, $Q_{12}=-0.016$ m^4/C^2, $Q_{44}=0.01$ m^4/C^2 $s_{11}=5.29\times10^{-12}$ m^2/N, $s_{12}=-1.85\times10^{-12}$ m^2/N, $s_{44}=1.47\times10^{-12}$ m^2/N
$SrTiO_3$ (STO) incipient ferroelectric	3 (without impurities)	Dielectric	${\varepsilon_{33}}^b=43$ (Ref. 38) ${\varepsilon_{33}}^b=5.7$ (Ref. 39) lattice constant $a=0.3905$ Å at room $\alpha_T=1.26\times10^6$ m/(F K) (Ref. 38) $T_c=38$ K, $T_q=84$ K, $\beta_b=(8.1-6.8\times10^9)$ $m^5/(C^2F)$, $\gamma=4\times10^{12}$ $m^9/(C^4F)$ (Refs. 39–41) $g=10^{-8}-10^{-9}$ m^3/F [below we used the value 0.99×10^{-9} m^3/F extracted from STEM data (Ref. 37)] $Q_{11}=0.051$ m^4/C^2, $Q_{12}=-0.016$ m^4/C^2, $Q_{44}=0.020$ m^4/C^2 $s_{11}=3.89\times10^{-12}$ m^2/N, $s_{12}=-1.06\times10^{-12}$ m^2/N, $s_{44}=8.20\times10^{-12}$ m^2/N

[a]Note that listed values of the LGD expansion coefficients account for the background permittivity contribution in accordance with relations $\alpha(T)=\varepsilon_0^{-1}[\varepsilon_{33}^{\exp}(T)-\varepsilon_{33}^b]^{-1}$ and $P_S^2=(\sqrt{\beta_b^2-4\alpha\gamma}-\beta_b)/2\gamma$, where $P_S^2(T)$ and $\varepsilon_{33}^{\exp}(T)$ are experimentally measured values.

in the screening interface charge. The characteristic feature of the interface charge absence is the thin depletion layer W_S (several nm for LSMO) that is occupied by the main-type carriers. The opposite case of depletion layers created by the minor-type carriers, which can appear during the polarization reversal in the proper ferroelectric film, will be considered in the next section.

D. Calculations of the metastable states for typical heterostructures (1D case)

As it was mentioned in Secs. II and III, when the free carriers are abundant there is no need in the screening interface charge (i.e., for thin depletion layer created by the main-type carriers and thick layer created by the minor-type carries). In the opposite case of depletion layers created only by

TABLE II. Renormalization of T_c^* and β by misfit stain and dislocations originated at critical film thickness h_d.

Interface (orientation)	u_m	h_d (nm)	T_c^* at $L\leq h_d$ $T_c+\frac{u_m}{\alpha_T}\frac{4Q_{12}}{s_{11}+s_{12}}$	T_c^* at $L>h_d$ $T_c+\frac{u_m}{\alpha_T}\frac{h_d}{L}\frac{4Q_{12}}{s_{11}+s_{12}}$	β at $L<h_d$ $\beta_b+\frac{4Q_{12}^2}{s_{11}+s_{12}}$	β at $L\gg h_d$ $\beta_b+\frac{4Q_{12}^2}{s_{11}+s_{12}}\frac{h_d^2}{L^2}$
LSMO/STO [100]	−0.0074	10.8	$-12T_c$	$T_c(1-13\frac{h_d}{L})$	$1.05\beta_b$	$\beta_b(1+0.05\frac{h_d^2}{L^2})$
LSMO/BFO [100]	−0.0230	2.4	$0.6T_c$	$T_c(1-0.4\frac{h_d}{L})$	$1.23\beta_b$	$\beta_b(1+0.23\frac{h_d^2}{L^2})$

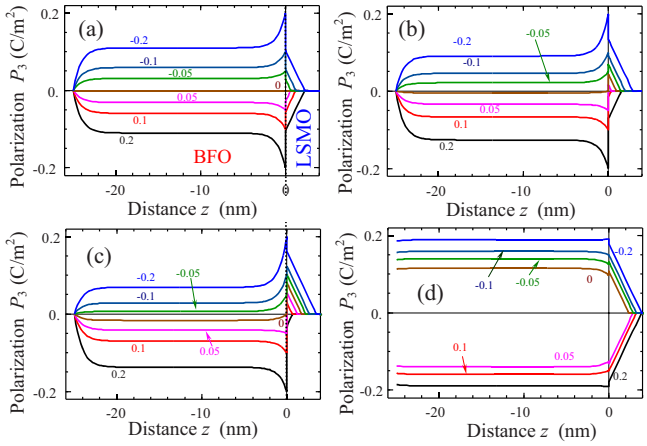

FIG. 3. (Color online) Polarization depth distribution (z in nm) for the BFO/LSMO heterostructure. Contact potential difference at $z=0$ is $U_b=0$ V, interface polarization $P_b=-0.2,-0.1,-0.05,0,0.05,0.1,0.2$ C/m^2 (curves from top to bottom). Carriers concentration in LSMO is $p_S^0=3\times10^{26}$ m^{-3}, BFO thickness $L=25$ nm. (a) Extrapolation lengths $\lambda_i=0$ nm and interface charge density $\sigma_S=0$; (b) $\sigma_S=0.05$ C/m^2 and $\lambda_i=0$ nm; (c) $\sigma_S=0.1$ C/m^2 and $\lambda_i=0$ nm; and (d) $\sigma_S=0$, $\lambda_1=5$ nm, and $\lambda_2=50$ nm.

the minor-type carriers (i.e., without interface charge states located at $z=0$) the penetration depth W_S is higher (up to tens of nanometers as shown by the bottom curves in Figs. 9) and corresponding screening of the spontaneous polarization appeared weaker (compare bottom curves in Fig. 9(a) for metastable polarization with the top curves for the stable ground state).

Figure 10 shows the hysteresis loops of the average polarization in the BFO film and corresponding field-penetration depth in LSMO under the absence of the interface charge σ_S and two different values of the major-type

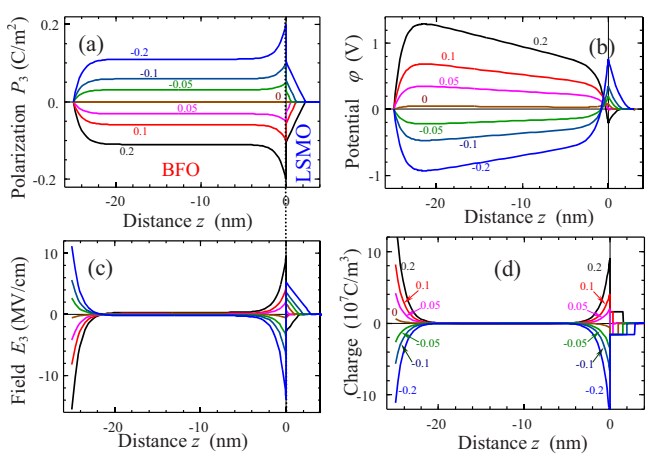

FIG. 4. (Color online) (a) Polarization, (b) potential, (c) electric field, and (d) electric charge density z distributions for the BFO/LSMO heterostructure. Contact potential difference at $z=0$ is $U_b=0$ V, interface charge density $\sigma_S=0.05$ C/m^2, and interface polarization $P_b=-0.3,-0.2,-0.1,0,0.1,0.2,0.3$ C/m^2 (curves from top to bottom). Carriers concentration in LSMO is $p_S^0=10^{26}$ m^{-3} and BFO thickness $L=25$ nm.

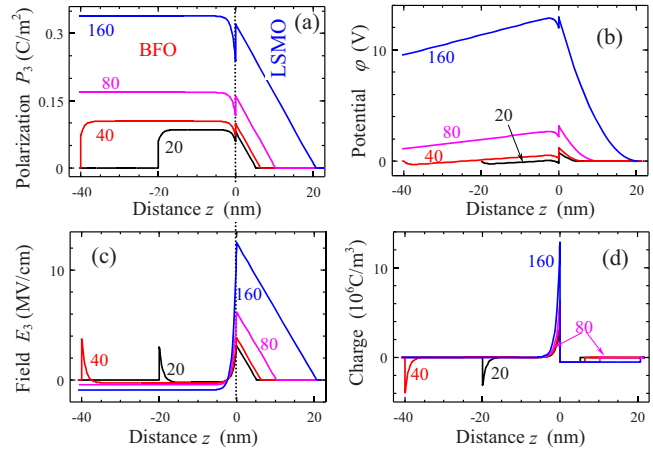

FIG. 5. (Color online) (a) Polarization, (b) potential, (c) electric field, and (d) electric charge density z distributions for the BFO/LSMO heterostructure. Contact potential difference at $z=0$ is $U_b=1$ V, interface polarization $P_b=0$ and charge density $\sigma_S=0$. Carriers concentration in LSMO is $p_S^0=10^{26}$ m^{-3}. Curves from the bottom to the top correspond to different values of BFO film thickness $L=20,40,80,160$ nm (figures near the curves) with extrapolation lengths $\lambda_i=2$ nm.

carriers in LSMO. The loops asymmetry increases with the increase in the carriers concentration [compare Figs. 10(a) and 10(c) with Figs. 10(b) and 10(d)]. The asymmetry of the loops, both horizontal imprint and vertical shift, are caused by the charge effects provided by the major-type carriers for positive biases $(U_e+U_b)>0$ and minor-type carriers for negative biases $(U_e+U_b)<0$, respectively, resulting in the appearance of the build-in field.

The weak screening causes strong electric fields, which resulting into the suppression of polarization inside the ferroelectric film and increase in the system's free energy since

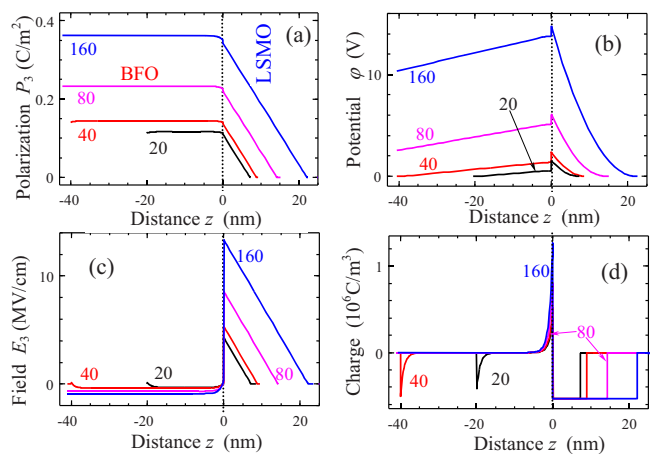

FIG. 6. (Color online) (a) Polarization, (b) potential, (c) electric field, and (d) electric charge density z distributions for the BFO/LSMO heterostructure. Contact potential difference at $z=0$ is $U_b=1$ V, interface polarization $P_b=0$, and charge density $\sigma_S=0$. Carriers concentration in LSMO is $p_S^0=10^{26}$ m^{-3}. Curves from the top to the bottom correspond to different thickness $L=20,40,80,160$ nm (figures near the curves) of BFO film with extrapolation lengths $\lambda_i=30$ nm.

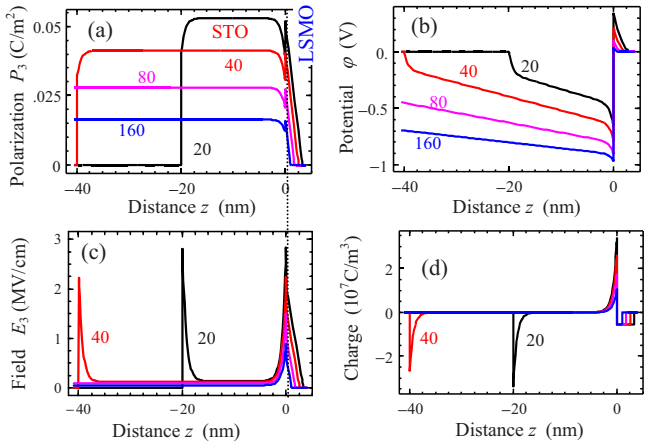

FIG. 7. (Color online) (a) Polarization, (b) potential, (c) electric field, and (d) electric charge density z distributions for the STO/LSMO heterostructure. Contact potential difference at $z=0$ is $U_b=1$ V, interface polarization $P_b=0$, and charge density $\sigma_S=0$. Carriers concentration in LSMO is $p_S^0=10^{26}$ m^{-3}. Curves from the top to the bottom correspond to different thickness $L=20,40,80,160$ nm (figures near the curves) of STO film with extrapolation lengths $\lambda_i \approx 2$ nm.

depolarization field energy is always positive. As a result, the strong field effect may lead to the bend bending at $z=0$ and appearance of interface charge states.

Figure 11 shows the influence of the interface charge on the thickness dependence of the stable and metastable (if any) states of the average polarization $\langle P_3 \rangle$ in ferroelectric BFO film. It is seen from Fig. 11 that the interface charges σ_S of appropriate sign increases the average polarization and smear the size-induced phase-transition point for the stable states (compare upper curves 1–5). Also the interface charges lead to the strong asymmetry of the average polarization values in the stable up and metastable down states, which exist

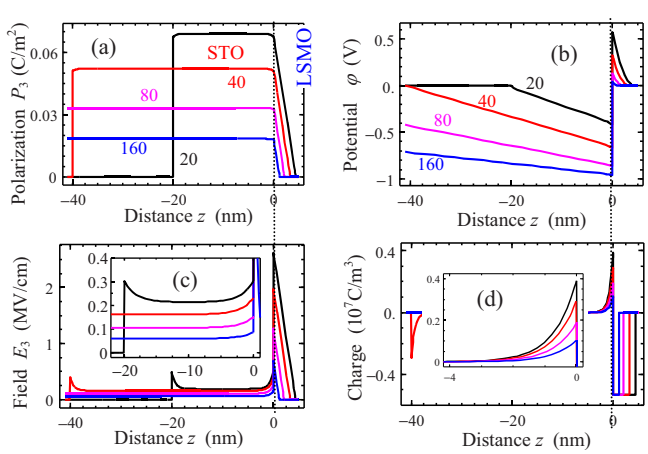

FIG. 8. (Color online) (a) Polarization, (b) potential, (c) electric field, and (d) electric charge density z distributions for the STO/LSMO heterostructure. Contact potential difference at $z=0$ is $U_b=1$ V, interface polarization $P_b=0$, and charge density $\sigma_S=0$. Carriers concentration in LSMO is $p_S^0=10^{26}$ m^{-3}. Curves from the top to the bottom correspond to different thickness $L=20,40,80,160$ nm (figures near the curves) of STO film with extrapolation lengths $\lambda_i=30$ nm.

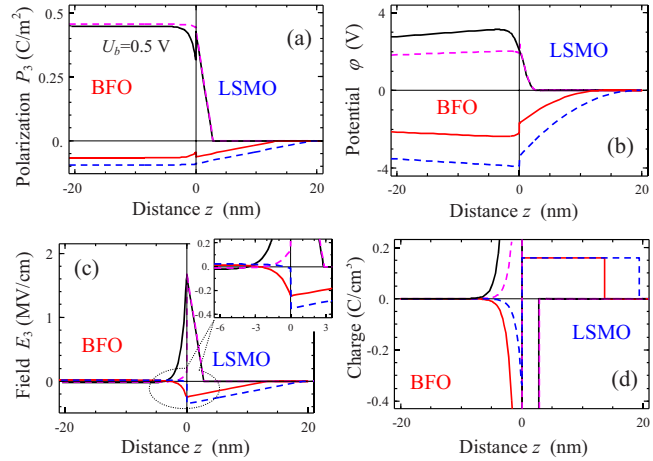

FIG. 9. (Color online) (a) Polarization, (b) potential, (c) electric field, and (d) bulk charge density z distributions near the BFO/LSMO interface at zero external bias $U_e=0$. Contact potential difference at $z=0$ is $U_b=0.5$ V, interface polarization $P_b=0$, and charge density $\sigma_S=0$. BFO film thickness $L=200$ nm, $\lambda_I=2$ nm (solid curves) and $\lambda_i=30$ nm (dashed curves). Carriers concentration in LSMO is $p_S^0=10^{27}$ m^{-3} (upper curves) and $n_S^0=3\times10^{25}$ m^{-3} (bottom curves). Upper curves (positive P_3) correspond to the stable ground states and bottom ones (negative P_3) correspond to the reversed polarization (metastable states).

not for all considered values of σ_S (compare up and bottom curves in Figs. 11). The interface charges σ_S act as the contribution into the built-in field in the right-hand side of Eqs. (10).

As expected, the interface charges σ_S of appropriate sign provide more effective screening of the spontaneous polarization than the extended space-charge layer. The screening by the interface charges σ_S makes polarization more homogeneous, subsequently decreases the depolarization field,

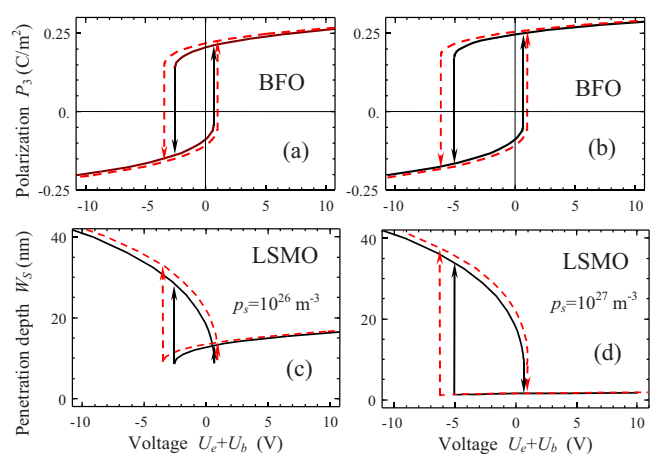

FIG. 10. (Color online) [(a) and (b)] Bias dependence of the average BFO polarization and [(c) and (d)] LSMO penetration depth. BFO film thickness $L=200$ nm and extrapolation lengths $\lambda_i=2$ nm (solid curves) and $\lambda_i=30$ nm (dashed curves). Interface polarization $P_b=0$ and charge density $\sigma_S=0$. [(a) and (c)] LSMO major-type carrier concentration is $p_S^0=10^{26}$ m^{-3} and $p_S^0=10^{27}$ m^{-3}, and [(b) and (d)] $n_S^0=3\times10^{25}$ m^{-3} for minor-type carriers respectively. Gap is absent ($H=0$).

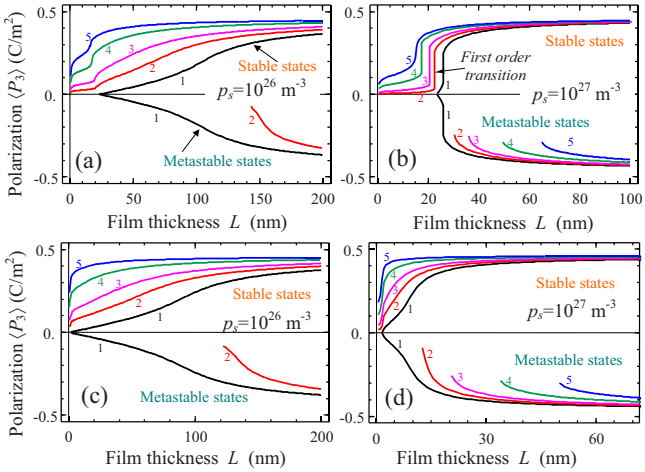

FIG. 11. (Color online) The average BFO polarization thickness dependence for different interface charge densities $\sigma_S=0,-0.05,-0.1,-0.2,-0.3$, C/m^2 (curves 1–5, respectively). Extrapolation lengths [(a) and (b)] $\lambda_i=3$ nm and [(c) and (d) $\lambda_i=20$ nm, carriers concentration in semiconductor is [(a) and (c)] $n_S^0=p_S^0=10^{26}$ m^{-3} and [(b) and (d)] $n_S^0=p_S^0=10^{27}$ m^{-3}. Other parameters are the same as in Figs. 9. Upper curves are the stable polarization states. Metastable states corresponding to negative polarization values are shown by the bottom curves (if any exist for definite σ_S).

which in turn self-consistently decreases the system free energy. So the absolutely stable profiles of reversed polarization shown in Fig. 12(a) by the bottom curves are more energetically preferable than the ones shown by the bottom curves in Fig. 9(a) for zero interface charges ($\sigma_S=0$). Thus the interface charge may originate in the case of the weak polarization screening from the semiconductor side (i.e., for thick depletion layer created by the minor-type carriers).

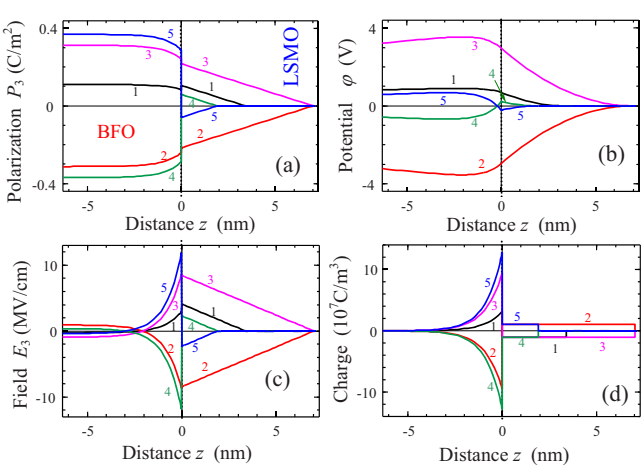

FIG. 12. (Color online) (a) Polarization, (b) potential, (c) electric field, and (d) electric charge density z distributions for the STO/LSMO heterostructure at zero external bias $U_e=0$. Contact potential difference at $z=0$ is $U_b=0$ V, interface polarization $P_b=0$, and different interface charge density $\sigma_S=0,+0.1,-0.1,+0.5,-0.5$ C/m^2 (curves 1–5, respectively). Carriers concentration in LSMO is $p_S^0=2\times10^{26}$ m^{-3}. BFO film thickness $L=50$ nm and extrapolation lengths $\lambda_i=3$ nm.

IV. EFFECT OF THE INCOMPLETE SCREENING AND INTERFACE CHARGE ON THE LOCAL POLARIZATION REVERSAL AND CHARGE TRANSPORT

In the initial (meta-) stable state the sluggish surface charges $\sigma_f=-\sigma_S+\rho_S^0W_S$ completely screen the electric displacement outside the film. In contrast to the ground states considered in the Sec. III, the recharging of surface charges σ_f should appear during the local polarization reversal. The ultrathin dielectric gap of thickness H models the separation between the tip electrode and the sluggish charges inside a contamination (or dead) layer.

The equilibrium domain structure is almost cylindrical for the case of local polarization reversal caused by the localized potential $U_e(x,y)$ applied to the SPM tip in thin ferroelectric film [Fig. 1(c)]. As a sequence the spontaneous polarization distribution, the potential and the interface charges density variations can be expressed in $\{x,y\}$-Fourier representation. In the Fourier $k_{1,2}$ domain Eqs. (2) and (3) immediately split into the two systems of differential equations. The first system corresponds to the smooth components $\{\varphi(z),P_3(z)\}$ was solved in the previous section. The second system for the modulating components is listed in Appendix B.

Approximate analytical solution in Eq. (6) may be used, in particular, case of the disklike tip apex of radius $R\gg L$, i.e., until $\Delta_\perp U_e(x,y)\approx0$ in the region of polarization reversal. It was shown earlier[44] that the transverse polarization gradient could be neglected for the case of the strong inequality $\sqrt{g/2|\alpha|}\ll R$ valid for all considered ferroelectrics at room temperature and $R>10$ nm. Thus polarization $P_3(x,y,z)\sim f(z,L)$ averaged over the film thickness can be determined from the Eqs. (10).

Using the coercive volume conception of polarization reversal formulated in Ref. 44, the domain lateral sizes $\{x,y\}$ can be estimated from the equation

$$\frac{\varepsilon_{33}^g\langle f\rangle}{\varepsilon_{33}^gL+\varepsilon_{33}^b(1-\mu)H}U_e(x,y)=E_c^{\pm}(L,H). \tag{15}$$

The intrinsic coercive fields are given by Eq. (11b) for the second-order ferroelectrics, $0<\mu<1$ is the dimensionless degree of the surface screening introduced earlier as $\sigma_f=\mu(\rho_S^0W_S-\sigma_S)$.

For a typical tip potential distribution $U_e(r)\approx\frac{Ud}{\sqrt{r^2+d^2}}$ (d is the effective tip size) the domain radius $r=\sqrt{x^2+y^2}$ depends on applied bias U as $r(U)=d\sqrt{U^2[\frac{\varepsilon_{33}^gL+\varepsilon_{33}^bH(1-\mu)}{\varepsilon_{33}^g\langle f\rangle}E_c^{\pm}]^{-2}-1}$.

In general, case the current density inside ferroelectric film consists of the conductivity, diffusion and displacement, tunneling, and Schottky and Frenkel-Poole emission currents.[45] During the local polarization reversal the thickness and electric charge of the space charge layer changes, in particular, the positive charge can be substituted by the negative one or vise versa depending on the polarization direction. Such transformations should be accompanied by the peaks of displacement currents, which shape and amplitude depend on the domain shape and sizes. However, for nanoscale contact a displacement current is significantly smaller and faster then a constant leakage current, and hence is ignored.

Derived analytical expressions also allow estimations of the tunneling current between the tip apex and ferroelectric surface (if any exist). Assuming that the ultrathin gap H is transparent for the tunneling electrons, tunneling and field emission currents could flow between the tip apex and ferroelectric film surface. In the Fowler-Nordheim transport regime[45,46] the tunneling current density $J_t(t) \sim E_3^2[\sigma_f(t)]\exp\{-\frac{2}{\hbar}\int_{-L-H}^{0}dz\sqrt{2m^*q|\varphi[z,\sigma_f(t)]-\varphi[0,\sigma_f(t)]|}\}$ is determined by the potential $\varphi(z,\sigma_f)$ and field $E_3[\sigma_f(t)]$ distributions given by Eqs. (6) and (7), and corresponding penetration depth in semiconductor, $W_S(U_e,L,H)$, is determined self-consistently from Eqs. (10). The determination of the surface-charge variation follows self-consistently from the continuity equation $\frac{\partial\sigma_f}{\partial t}=-J_t$ supplemented by the initial condition, e.g., $\sigma_f(t=0)=0$.

V. SUMMARY

Using Landau-Ginzburg-Devonshire approach we have calculated the equilibrium distributions of electric field, polarization, and space charge in the ferroelectric-semiconductor heterostructures containing proper or incipient ferroelectric thin films. In particular, it is shown that space-charge effects introduce strong size effect on spontaneous polarization in 20–40-nm epitaxial films of ferroelectric $BiFeO_3$ on half-metal $(La,Sr)MnO_3$ substrate, and can induce strong polarization in incipient ferroelectric $SrTiO_3$ on $(La,Sr)MnO_3$.

We obtained analytical expressions for the cylindrical domain sizes appeared in ferroelectric film under the local polarization reversal, which is caused by the electric field induced by the nanosized tip of the SPM probe. The intrinsic field effects, which originated at the ferroelectric-semiconductor interface, lead to the surface band bending and result in the formation of the space-charge layer near the semiconductor surface. We calculated how the build-in fields smear the size-induced phase transition, induce polarization in the incipient ferroelectric films, and lead to the polarization hysteresis loops vertical and horizontal asymmetry in ferroelectric films. Derived analytical expressions allow estimations of the tunneling current between the tip apex and ferroelectric surface.

ACKNOWLEDGMENTS

Authors are grateful to E. Tsymbal and E. Tsymbal for valuable critical remarks. Research is sponsored by Ministry of Science and Education of Ukraine and National Science Foundation (Materials World Network, Grant No. DMR-0908718). S.V.K. and A.B. acknowledge the DOE SISGR program. P.M. is supported by the Division of Scientific User Facilities, US DOE.

APPENDIX A: POLARIZATION DISTRIBUTION CALCULATION

Allowing for Eq. (7), polarization distribution $P_3(z)$ should be found from the Euler-Lagrange boundary problem in Eq. (2) as

$$\begin{cases} \left(\alpha+\dfrac{1}{\varepsilon_0\varepsilon_{33}^b}\right)P_3+\beta P_3^3+\gamma P_3^5-g\dfrac{d^2}{dz^2}P_3=\dfrac{\rho_S^0W_S-\sigma_S}{\varepsilon_0\varepsilon_{33}^b} \\ \left(P_3+\lambda_1\dfrac{dP_3}{dz}\right)\Big|_{z=0}=-P_b, \quad \left(P_3-\lambda_2\dfrac{dP_3}{dz}\right)\Big|_{z=-L}=0. \end{cases} \tag{A1}$$

Let us look for the solution of the problem (A1) in the form $P_3(z)=\langle P_3\rangle+p(z)$, where the average polarization $\langle P_3\rangle \equiv \frac{1}{L}\int_{-L}^{0}P_3(\tilde{z})d\tilde{z}$ is introduced. The variation p average value is zero: $\langle p\rangle\equiv 0$. So, the problem (A1) acquires the form

$$\begin{cases} \left(\alpha+3\beta\langle P_3\rangle^2+5\gamma\langle P_3\rangle^4+\dfrac{1}{\varepsilon_0\varepsilon_{33}^b}\right)p+3\beta\langle P_3\rangle p^2+\beta p^3-g\dfrac{d^2p}{dz^2} \\ =\dfrac{\rho_S^0W_S-\sigma_S-\langle P_3\rangle}{\varepsilon_0\varepsilon_{33}^b}-(\alpha\langle P_3\rangle+\beta\langle P_3\rangle^3+\gamma\langle P_3\rangle^5) \\ \left(p+\lambda_1\dfrac{dp}{dz}\right)\Big|_{z=0}=-\langle P_3\rangle-P_b, \quad \left(p-\lambda_2\dfrac{dp}{dz}\right)\Big|_{z=-L}=-\langle P_3\rangle. \end{cases} \tag{A2}$$

Since always $\alpha+\frac{1}{\varepsilon_0\varepsilon_{33}^b}\gg 0$ (as well as $\alpha+3\beta\langle P_3\rangle^2+\frac{1}{\varepsilon_0\varepsilon_{33}^b}\gg 0$) for both proper and incipient ferroelectrics, Eq. (A2) can be linearized with respect to the deviation p and then solved by standard methods.

After elementary transformations, polarization distribution acquires the form

$$P_3(z)=\frac{\varepsilon_S-1}{\varepsilon_S}q\begin{cases} p_S^0(z-W_{Sp})\cdot\theta(W_{Sp}-z), & z\geq 0, \quad \text{depletion of } n\text{-type carriers} \\ -n_S^0(z-W_{Sn})\cdot\theta(W_{Sn}-z), & z\geq 0, \quad \text{depletion of } p\text{-type carriers,} \end{cases} \tag{A3}$$

$$P_3(z) = \frac{2\varepsilon_0\varepsilon_{33}^b\langle P_3\rangle^3(\beta + 2\gamma\langle P_3\rangle^2) + \rho_S^0 W_S - \sigma_S}{\varepsilon_0\varepsilon_{33}^b(\alpha + 3\beta\langle P_3\rangle^2) + 1} f(z,L) - P_b b(z,L), \quad -L < z \leq 0. \tag{A4}$$

The space distribution is governed by the functions f and b

$$f(z,L) = 1 - \xi\frac{\lambda_2 \cosh[(L+z)/\xi] + \lambda_1 \cosh(z/\xi) + \xi\{\sinh[(L+z)/\xi] - \sinh(z/\xi)\}}{(\xi^2 + \lambda_1\lambda_2)\sinh(L/\xi) + \xi(\lambda_1 + \lambda_2)\cosh(L/\xi)}, \tag{A5a}$$

$$b(z,L) = \frac{\xi\lambda_2 \cosh[(L+z)/\xi] + \xi^2 \sinh[(L+z)/\xi]}{(\xi^2 + \lambda_1\lambda_2)\sinh(L/\xi) + \xi(\lambda_1 + \lambda_2)\cosh(L/\xi)}. \tag{A5b}$$

Characteristic length

$$\xi = \sqrt{\frac{\varepsilon_0\varepsilon_{33}^b g}{\varepsilon_0\varepsilon_{33}^b(\alpha + 3\beta\langle P_3\rangle^2 + 5\gamma\langle P_3\rangle^4) + 1}} \approx \sqrt{\varepsilon_0\varepsilon_{33}^b g}.$$

Then the average polarization $\langle P_3\rangle$ and depths $W_{Sn,p}$ should be determined self-consistently from the spatial averaging of Eq. (8b), $\langle P_3\rangle = \frac{2\varepsilon_0\varepsilon_{33}^b\langle P_3\rangle^3(\beta+2\gamma\langle P_3\rangle^2)+\rho_S^0 W_S-\sigma_S}{\varepsilon_0\varepsilon_{33}^b(\alpha+3\beta\langle P_3\rangle^2+5\gamma\langle P_3\rangle^4)+1}\langle f\rangle - P_b\cdot\langle b\rangle$, and boundary conditions in Eqs. (4b) and (4c).

For particular case $H=0$ and $\gamma=0$, $\beta>0$ for the second-order ferroelectrics this gives the system of coupled algebraic equations

$$\begin{cases} -\dfrac{\rho_S^0 W_S^2}{2\varepsilon_0\varepsilon_S} + L\left(\dfrac{\rho_S^0 W_S}{\varepsilon_0\varepsilon_{33}^b} - \dfrac{\sigma_S + \langle P_3\rangle}{\varepsilon_0\varepsilon_{33}^b}\right) = U_b \\ \langle P_3\rangle\left(\alpha + \beta\langle P_3\rangle^2(3 - 2\langle f\rangle) + \dfrac{1}{\varepsilon_0\varepsilon_{33}^b}\right) = \left(\dfrac{\rho_S^0 W_S - \sigma_S}{\varepsilon_0\varepsilon_{33}^b}\right)\langle f\rangle - P_b\langle b\rangle\left(\alpha + 3\beta\langle P_3\rangle^2 + \dfrac{1}{\varepsilon_0\varepsilon_{33}^b}\right), \end{cases} \tag{A6}$$

where

$$\langle f\rangle = 1 - \frac{\xi^2\{2\xi[\cosh(L/\xi) - 1] + (\lambda_1 + \lambda_2)\sinh(L/\xi)\}}{L[\xi(\lambda_1 + \lambda_2)\cosh(L/\xi) + (\xi^2 + \lambda_1\lambda_2)\sinh(L/\xi)]} \approx 1 - \frac{\xi^2(2\xi + \lambda_1 + \lambda_2)}{L[\xi(\lambda_1 + \lambda_2) + \xi^2 + \lambda_1\lambda_2]}$$

and

$$\langle b\rangle = \frac{\xi^2\lambda_2 \sinh(L/\xi) - \xi^3[1 - \cosh(L/\xi)]}{L[(\xi^2 + \lambda_1\lambda_2)\sinh(L/\xi) + \xi(\lambda_1 + \lambda_2)\cosh(L/\xi)]} \approx \frac{\xi^2(\xi + \lambda_2)}{L[\xi^2 + \lambda_1\lambda_2 + \xi(\lambda_1 + \lambda_2)]} = \frac{\xi^2}{L(\xi + \lambda_1)}..$$

The system (A6) reduces to the relations

$$\begin{cases} \langle P_3\rangle = -\sigma_S + \rho_S^0 W_S + \dfrac{\varepsilon_{33}^b\rho_S^0}{2L\varepsilon_S} W_S^2 - \varepsilon_0\varepsilon_{33}^b\dfrac{U_b}{L} \\ \left(\alpha + \dfrac{1}{\varepsilon_0\varepsilon_{33}^b}\right)\langle P_3\rangle + \beta\langle P_3\rangle^3(3 - 2\langle f\rangle) = \left(\dfrac{\rho_S^0 W_S - \sigma_S}{\varepsilon_0\varepsilon_{33}^b}\right)\langle f\rangle - \dfrac{P_b\langle b\rangle}{\varepsilon_0\varepsilon_{33}^b}. \end{cases} \tag{A7}$$

Since $\langle P_3\rangle = -\sigma_S + \rho_S^0 W_S + \frac{\varepsilon_{33}^b \rho_S^0}{2L\varepsilon_S} W_S^2 - \varepsilon_0 \varepsilon_{33}^b \frac{U_b}{L}$ and $(\langle P_3\rangle + \sigma_S + \varepsilon_0 \varepsilon_{33}^b \frac{U_b}{L}) \frac{1}{\rho_S^0} > 0$, the second of Eqs. (14) reduces to six-order algebraic equation for the built-in field determination.

The polarization contribution into the relative atomic displacement u_3 can be estimated as $u_3(z) \approx \frac{V_S}{Q_S^B} P_3(z)$ at $z>0$ and $u_3(z) \approx \frac{V_{FE}}{Q_{IF}^B} P_3(z)$ at $-L<z<0$. Here V_j is the volume of the corresponding unit cell, Q^B is the Born effective charge of the lightest atom "B." For perovskites considered hereinafter $V_{FE,S} \approx 6.4 \times 10^{-29}$ m^3

APPENDIX B: CALCULATIONS OF LOCAL SWITCHING INDUCED BY SPM TIP

The potential applied to the SPM tip is localized, i.e., $U(x,y) = \int_{-\infty}^{\infty} dk_1 \int_{-\infty}^{\infty} dk_2 u(\mathbf{k}) \exp(-ik_1 x - ik_2 y)$. As a sequence the spontaneous polarization distribution can be approximated as $P_S(x,y,z) = P_3(z) + \int_{-\infty}^{\infty} dk_1 \int_{-\infty}^{\infty} dk_2 p_S(\mathbf{k},z) \exp(-ik_1 x - ik_2 y)$, the potential $\varphi_f(x,y,z) = \varphi(z) + \int_{-\infty}^{\infty} dk_1 \int_{-\infty}^{\infty} dk_2 \tilde{\varphi}(\mathbf{k},z) \exp(-ik_1 x - ik_2 y)$ and the interface charges density variation $\delta\sigma_S(x,y) = \int_{-\infty}^{\infty} dk_1 \int_{-\infty}^{\infty} dk_2 \tilde{\sigma}_S(\mathbf{k}) \exp(-ik_1 x - ik_2 y)$ can be expressed in Fourier representation.

In the Fourier $k_{1,2}$ domain Eqs. (3) immediately split into the two systems of differential equations. The first system corresponds to the smooth components $\{\varphi(z), P_3(z)\}$ was solved in the previous section. The second system for the modulating components is

$$\frac{d^2\tilde{\varphi}}{dz^2} - k^2\tilde{\varphi} = 0, \quad -H-L<z<-L,$$

$$\varepsilon_{33}^b \frac{d^2\tilde{\varphi}}{dz^2} - \varepsilon_{11} k^2 \tilde{\varphi} = \frac{1}{\varepsilon_0} \frac{dp_S(\mathbf{k},z)}{dz}, \quad -L<z<0,$$

$$\frac{d^2\tilde{\varphi}}{dz^2} - k^2\tilde{\varphi} = 0, \quad z>0, \tag{B1}$$

where $k^2 = k_1^2 + k_2^2$. Rewritten for the modulating components, the boundary conditions in Eq. (4) acquire the form

$$\tilde{\varphi}(k,-L-H) = u(k),$$

$$\tilde{\varphi}(k,-L+0) - \tilde{\varphi}(k,-L-0) \approx 0,$$

$$\varepsilon_0 \left[\varepsilon_{33}^b \frac{d\tilde{\varphi}(k,-L+0)}{dz} - \varepsilon_{33}^g \frac{d\tilde{\varphi}(k,-L-0)}{dz} \right] - p_S(k,-L) = \tilde{\sigma}_f(\mathbf{k}),$$

$$\varepsilon_0 \left[\varepsilon_{33}^b \frac{d\tilde{\varphi}(k,+0)}{dz} - \varepsilon_S \frac{d\tilde{\varphi}(k,-0)}{dz} \right] - p_S(k,0) = \tilde{\sigma}_S(\mathbf{k}),$$

$$\tilde{\varphi}(k,+0) - \tilde{\varphi}(k,-0) \approx 0,$$

$$\tilde{\varphi}(k,z\to\infty) = 0, \tag{B2}$$

where the gap dielectric permittivity ε_{33}^g is introduced.

LGD equation, Eq. (2), for determination of the modulation $p_S(\mathbf{k},z)$ acquires the form

$$\left[\alpha + gk^2 + 3\beta P_3^2(z) - g\frac{d^2}{dz^2} \right] p_S(\mathbf{k},z) = -\frac{d}{dz}\tilde{\varphi}(\mathbf{k},z) - \beta Q[p_S(\mathbf{k},z)],$$

$$Q[p_S(\mathbf{k},z)] = \int_{-\infty}^{\infty} d\mathbf{k}' p_S(\mathbf{k}') \int_{-\infty}^{\infty} d\mathbf{k}'' p_S(\mathbf{k}-\mathbf{k}'-\mathbf{k}'') p_S(\mathbf{k}'') + 3P_3(z) \int_{-\infty}^{\infty} d\mathbf{k}' p_S(\mathbf{k}-\mathbf{k}') p_S(\mathbf{k}').$$

$$\left(p_S + \lambda_1 \frac{dp_S}{dz} \right)\Big|_{z=0} = 0, \quad \left(p_S - \lambda_2 \frac{dp_S}{dz} \right)\Big|_{z=-L} = 0 \tag{B3}$$

The value $p_S(\mathbf{k},-L)$ should be determined self-consistently allowing for the distribution of the surface charge $\tilde{\sigma}_f(\mathbf{k})$ localized at $z=-L$ and the interface charge $\tilde{\sigma}_S(\mathbf{k})$ localized at $z=0$.

*morozo@i.com.ua
†sergei2@ornl.gov

[1] A. Ohtomo, D. A. Muller, J. L. Grazul, and H. Y. Hwang, Nature (London) **419**, 378 (2002).
[2] A. Ohtomo and H. Y. Hwang, Nature (London) **427**, 423 (2004).
[3] H. Y. Hwang, MRS Bull. **31**, 28 (2006).
[4] S. Okamoto and A. J. Millis, Nature (London) **428**, 630 (2004).
[5] R. G. Moore, J. Zhang, V. B. Nascimento, R. Jin, J. Guo, G. T. Wang, Z. Fang, D. Mandrus, and E. W. Plummer, Science **318**, 615 (2007).
[6] V. Garcia, S. Fusil, K. Bouzehouane, S. Enouz-Vedrenne, N. D. Mathur, A. Barthélémy, and M. Bibes, Nature (London) **460**, 81 (2009).
[7] P. Maksymovych, S. Jesse, Yu. Pu, R. Ramesh, A. P. Baddorf, and S. V. Kalinin, Science **324**, 1421 (2009).
[8] A. Gruverman, D. Wu, H. Lu, Y. Wang, H. W. Jang, C. M. Folkman, M. Ye. Zhuravlev, D. Felker, M. Rzchowski, C.-B. Eom, and E. Y. Tsymbal, Nano Lett. **9**, 3539 (2009).
[9] T. Choi, S. Lee, Y. J. Choi, V. Kiryukhin, and S.-W. Cheong, Science **324**, 63 (2009).
[10] J. F. Scott, *Ferroelectric Memories*, Springer Series in Advanced Microelectronics Vol. 3, (Springer-Verlag, Berlin, 2000), p. 248.
[11] P. W. M. Blom, R. M. Wolf, J. F. M. Cillessen, and M. P. C. M. Krijn, Phys. Rev. Lett. **73**, 2107 (1994).
[12] P. Zubko, D. J. Jung, and J. F. Scott, J. Appl. Phys. **100**, 114112 (2006).
[13] P. Zubko, D. J. Jung, and J. F. Scott, J. Appl. Phys. **100**, 114113 (2006).
[14] Y. Watanabe, Phys. Rev. B **57**, 789 (1998).
[15] J. Bardeen, Phys. Rev. **71**, 717 (1947).

[16] V. M. Fridkin, *Ferroelectrics Semiconductors* (Consultant Bureau, New York, London, 1980), p. 119.
[17] M. A. Itskovsky, Fiz. Tverd. Tela (Leningrad) **16**, 2065 (1974).
[18] The dependence of ε_{11} on E_3 is absent for uniaxial ferroelectrics. It may be essential for perovskites with high coupling constant.
[19] C.-G. Duan, R. F. Sabirianov, W.-N. Mei, S. S. Jaswal, and E. Y. Tsymbal, Nano Lett. **6**, 483 (2006).
[20] C.-G. Duan, S. S. Jaswal, and E. Y. Tsymbal, Phys. Rev. Lett. **97**, 047201 (2006).
[21] M. D. Glinchuk and A. N. Morozovska, J. Phys.: Condens. Matter **16**, 3517 (2004).
[22] M. D. Glinchuk, A. N. Morozovska, and E. A. Eliseev, J. Appl. Phys. **99**, 114102 (2006).
[23] S. M. Sze, *Physics of Semiconductor Devices*, 2nd ed. (Wiley-Interscience, New York, 1981), Chap. 7, p. 382.
[24] S. Ducharme, V. M. Fridkin, A. V. Bune, S. P. Palto, L. M. Blinov, N. N. Petukhova, and S. G. Yudin, Phys. Rev. Lett. **84**, 175 (2000).
[25] A. K. Tagantsev, G. Gerra, and N. Setter, Phys. Rev. B **77**, 174111 (2008).
[26] N. A. Pertsev, A. G. Zembilgotov, and A. K. Tagantsev, Phys. Rev. Lett. **80**, 1988 (1998).
[27] J. S. Speck and W. J. Pompe, J. Appl. Phys. **76**, 466 (1994).
[28] E. A. Eliseev, M. D. Glinchuk, and A. N. Morozovska, Phys. Status Solidi B **244**, 3660 (2007).
[29] T. Muramatsu, Y. Muraoka, and Z. Hiroi, Solid State Commun. **132**, 351 (2004).
[30] J. Kui-juan, L. Hui-bin, Z. Qing-li, K. Zhao, C. Bo-lin, C. Zheng-hao, Z. Yue-liang, and G.-Z. Yang, Phys. Rev. B **71**, 184428 (2005).
[31] A. Tiwari, C. Jin, D. Kumar, and J. Narayan, Appl. Phys. Lett. **83**, 1773 (2003).
[32] A. Ruotolo, C. Y. Lam, W. F. Cheng, K. H. Wong, and C. W. Leung, Phys. Rev. B **76**, 075122 (2007).
[33] J. L. Cohn, M. Peterca, and J. J. Neumeier, Phys. Rev. B **70**, 214433 (2004).
[34] R. P. S. M. Lobo, R. L. Moreira, D. Lebeugle, and D. Colson, Phys. Rev. B **76**, 172105 (2007).
[35] G. Catalan and J. F. Scott, Adv. Mater. **21**, 2463 (2009).
[36] J. X. Zhang, Y. L. Li, Y. Wang, Z. K. Liu, L. Q. Chen, Y. H. Chu, F. Zavaliche, and R. Ramesh, J. Appl. Phys. **101**, 114105 (2007).
[37] A. Y. Borisevich *et al.*, Direct mapping of interface electric fields from STEM atomic positions (unpublished).
[38] G. A. Smolenskii, V. A. Bokov, V. A. Isupov, N. N. Krainik, R. E. Pasynkov, and A. I. Sokolov, *Ferroelectrics and Related Materials* (Gordon and Breach, New York, 1984), p. 421.
[39] P. A. Fleury and J. M. Worlock, Phys. Rev. **174**, 613 (1968).
[40] Y. L. Li, S. Choudhury, J. H. Haeni, M. D. Biegalski, A. Vasudevarao, A. Sharan, H. Z. Ma, J. Levy, V. Gopalan, S. Trolier-McKinstry, D. G. Schlom, Q. X. Jia, and L. Q. Chen, Phys. Rev. B **73**, 184112 (2006).
[41] N. A. Pertsev, A. K. Tagantsev, and N. Setter, Phys. Rev. B **61**, R825 (2000).
[42] C.-L. Jia, V. Nagarajan, J.-Q. He, L. Houben, T. Zhao, R. Ramesh, K. Urban, and R. Waser, Nature Mater. **6**, 64 (2007).
[43] M. D. Glinchuk, E. A. Eliseev, A. Deineka, L. Jastrabik, G. Suchaneck, T. Sandner, G. Gerlach, and M. Hrabovsky, Integr. Ferroelectr. **38**, 101 (2001).
[44] A. N. Morozovska, E. A. Eliseev, Y. Li, S. V. Svechnikov, P. Maksymovych, V. Y. Shur, V. Gopalan, L.-Q. Chen, and S. V. Kalinin. Phys. Rev. B **80**, 214110 (2009).
[45] M. Grossmann, O. Lohse, D. Bolten, U. Boettger, and R. Waser, J. Appl. Phys. **92**, 2688 (2002).
[46] I. C. Infante, F. Sanchez, V. Laukhin, A. Perez del Pino, J. Fontcuberta, K. Bouzehouane, S. Fusil, and A. Barthelemy, Appl. Phys. Lett. **89**, 172506 (2006).